3D Topography Effects on Amplification of Plane Harmonic Body and Surface Waves

B. Omidvar [1*], M. Rahimian [2], T. Mohammadnejad [3], and A.R. Sanaeiha [4]

1. Assistant Professor, Faculty of Environment, University of Tehran, I.R. Iran
* Corresponding Author; email: bomidvar@ut.ac.ir
2. Professor, Faculty of Civil Engineering, University of Tehran, I.R. Iran
3. PhD Student, Department of Civil Engineering, Sharif University of Technology, I.R. Iran
4. PhD Student, Faculty of Civil Engineering, University of Tehran, I.R. Iran

ABSTRACT

In this paper, three-dimensional scattering of plane harmonic SH, SV, P, and Rayleigh waves by surface topographies is investigated by using a boundary element method in frequency domain. It is shown that for exact evaluation of surface ground motions in topographies all efficient parameters such as geometry of the region, mechanical properties of the surrounding geological materials (density, Poisson's ratio, and shear modulus), wave type, azimuth and angle of incidence, as well as stimulation frequency must be taken into account altogether. Furthermore, the results emphasize the need for three-dimensional modeling of irregularities. Most of the topographies in the nature are composed from the simple shape. Based on this fact, four problems are considered in order to study the effects of the shape of the topography on the surface ground motion amplification. In order to assess the accuracy and efficiency of the proposed formulations for the computation of the surface displacement field amplification, several problems are considered. The investigated problems are hemispherical canyons, elliptical-shaped canyons, hemispherical hills and rectangular cube canyons.

Keywords:
Boundary element method; Body and surface wave; Wave Propagation; Topographic effect; Frequency domain

1. Introduction

It has long been found that the effects of topography can significantly affect the nature of strong ground motion during earthquakes [1-2]. In some situations, ground motion amplification can adequately be inferred using simple one-dimensional models. However, due to lateral variations, the problem must be dealt with as a spatial phenomenon. Local conditions can generate large amplifications and important spatial variations of seismic ground motion. Certainly, in the recent past, there have been numerous cases of recorded motions and observed earthquake damage pointing towards topographic amplification as an important effect. Indeed, it has been often reported, after destructive earthquakes in mountain areas, that buildings located at the top of cliffs or hills suffer much more intensive damage than those located at the base. For example, the 1968 Tokachi-oki earthquake in Japan produced considerable damage to buildings close to the edge of a cliff; whereas buildings located relatively far from the edge did not present any damage. High accelerations were recorded at the Pacoima Dam (1.25*g*) during the San Fernando, California earthquake of February 9, 1971 [3-4]. For the aftershocks of the same earthquake, Davis and West [5] in a series of observations have found significant local amplifications due to topographical relief. In particular, local irregularities can be relevant in calculating the seismic response of long structures like dams, bridges or life-line systems [6]. The site amplification effects have been the subject of numerous experimental and theoretical studies. Since 1973, when Trifunac [7] initiated theoretical work on the two-dimensional response of a semicircular canyon subjected to harmonic *SH*-wave excitation, a great deal of work has been done to study the site effects on strong ground motions

[8-23]. Still, there are very few theoretical investigations for three-dimensional problems of this type. Most of the papers that have appeared in the literature are limited to simple geometries and axisymmetric cases. Lee [24] investigated diffraction of elastic plane *P*, *SV*, and *SH* waves by a hemispherical canyon using the method of series expansion. Sanchez-Sesma [25] considered diffraction of a vertical incident *P* wave by several types of irregularities including canyon and alluvial basins using the c-complete family of wave functions. Both studies were limited to axisymmetric cases. Sneider [26] used the Born approximation to study the effect of topography on three-dimensional surface wave scattering. Such an approximation is valid only for long period waves and topographies with shallow slopes. Mossessian and Dravinski [27] have applied an indirect boundary integral equation method to study the amplification of elastic waves by three-dimensional canyons of arbitrary shape. Reinoso et al [28] have presented a direct boundary element method for calculating the three-dimensional scattering of seismic waves from irregular topographies and buried valleys due to incident *P*-, *S*- and Rayleigh waves. Omidvar et al [29] have studied three-dimensional scattering of plane harmonic *SH*, *SV*, and *P* waves in multilayered alluvial valleys. Gatmiri and Arson [30-31] have studied seismic site effects by an optimized 2*D BE/FE* method.

Several studies including site response analysis of half-plane, horizontally layered sites, canyons, alluvial valleys and ridge sections subjected to incident *P* and *SV* waves were done in time domain [32-33]. An extensive numerical parametric study on seismic behavior of two-dimensional semi-sine-shaped valleys subjected to vertically propagating incident in-plane waves has been investigated by Kamalian et al [34]. They have shown that wavelength, site geometry and in a less order of importance, wave type and material parameters, are the independent key parameters governing the valley's amplification pattern. Also, they demonstrated that in incidence of waves with wavelengths longer than the width of the hill, the amplification curve usually finds its maximum at the crest and decreases towards the base of the hill. Some de-amplification zones would occur along the hill as well [35-36].

The boundary element algorithm that uses the presented time-convoluted traction kernels is applied to site response analyses of topographic structures by Sohrabi-Bidar et al [37]. They concluded that seismic response analyses of three-dimensional Gaussian-shaped ridges show that the three-dimensional axisymmetric ridge has a more amplification potential compared with three-dimensional non-axisymmetric elongated and two-dimensional ridges, if the ridge is impinged by incident waves with wavelength of about the ridge's width.

Recently, Lee et al [38] have demonstrated the effects of topography on seismic-wave propagation by developing a new spectral-element mesh implementation to accommodate realistic topography. As it said, because of the complexity of such problems, closed form of analytical solutions are not available for complex topography. However, recent advances in computational techniques have made numerical approaches more feasible for practical problems. Boundary element method (*BEM*) is one of such approaches. This technique formulates the problem in terms of boundary values. The main advantage of *BEM*, especially in comparison with finite element and finite difference methods, is that the discretization is only applied to the boundary, thus reducing the volume of modeling and the number of unknown variables. Moreover, the radiation condition at infinity is completely satisfied in this method which is very prominent for wave propagation problems. The aim of this work is to study the problem of calculating the 3*D* effects of topographical and geological irregularities on ground motion using *BEM* in frequency domain. Three-dimensional scattering of plane harmonic *SH*, *SV*, *P*, and Rayleigh waves by surface topographies is investigated in a parametric study. The investigated problems in the paper are all analyzed using boundary-element software which is improved by the authors.

2. Propagation of Plane Harmonic Waves in a Half-Space

Consider Ω as a homogeneous and linearly elastic three-dimensional half-space under the boundary Γ at $y = 0$. The propagation of plane harmonic waves in domain Ω is described by the Navier-Cauchy equation. For time-harmonic problems, with the dependence on time as exp ($i\omega t$), the Navier-Cauchy equation is as follows:

$$c_2^2\nabla^2\mathbf{u} + (c_1^2 - c_2^2)\nabla(\nabla.\mathbf{u}) + \omega^2\mathbf{u} = 0 \qquad (1)$$

where

$$c_1 = (\frac{\lambda + 2\mu}{\rho})^{1/2} \; ; \; c_2 = (\frac{\mu}{\rho})^{1/2} \tag{2}$$

are the longitudinal and transversal wave velocities, respectively. ω is the circular frequency of the incident wave and **u** is the displacement vector. The solution of the Navier-Cauchy equation has to satisfy the traction-free boundary condition at the boundary Γ.

One method of solving Eq. (1) is to use potential functions. According to Helmholtz theorem, the displacement field u can be expressed as the sum of the gradient of a scalar field φ, plus the curl of a vector field y, i.e.

$$\mathbf{u} = \nabla\varphi + \nabla \times \mathrm{y} \tag{3}$$

y must be such that the relation $\nabla.\mathrm{y} = 0$ is satisfied. The displacement field in the form of Eq. (3) satisfies the Navier-Cauchy equation if the potential functions satisfy the following equations:

$$\begin{aligned} &\nabla^2\varphi + k_1^2\,\varphi = 0 \\ &\nabla^2\psi_k + k_2^2\,\psi_k = 0 \end{aligned} \tag{4}$$

with $k_1 = \omega/c_1$ and $k_2 = \omega/c_2$ the longitudinal and transversal wave numbers, respectively. Eqs. (4) are called the Helmholtz equations or the wave equations in the frequency domain (reduced wave equations).

Assume that the plane waves travel in the $x' - y'$ plane, so it is yielded $\frac{\partial}{\partial z'} = 0$. By using the Helmholtz decomposition, the in-plane displacements u' and v' are given as:

$$\begin{aligned} u' &= \frac{\partial\varphi}{\partial x'} + \frac{\partial\psi}{\partial y'} \\ v' &= \frac{\partial\varphi}{\partial y'} - \frac{\partial\psi}{\partial x'} \end{aligned} \tag{5}$$

while the out-of-plane displacement ω′ is as follows:

$$\omega' = \frac{\partial\psi_2}{\partial x'} - \frac{\partial\psi_1}{\partial y'} \tag{6}$$

Consider the reference coordinate system *x*, *y* and *z*. In the general case that normal to the wave front, i.e. the wave propagation direction, lies in the $x' - y'(y' = y)$ plane, see Figure (1), where the plane

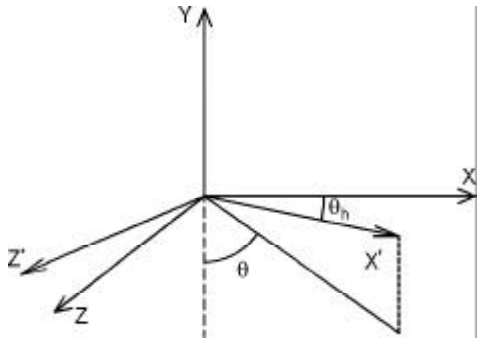

Figure 1. Position of the propagation wave plane $x' - y'(y' = y)$ relative to the reference coordinate system x - y - z.

forms a horizontal incidence angle with respect to the general plane, the displacements in the general system are obtained by using the following transformation matrix as follows:

$$\begin{Bmatrix} u \\ v \\ \omega \end{Bmatrix} = \begin{bmatrix} \cos\theta_h & 0 & -\sin\theta_h \\ 0 & 1 & 0 \\ \sin\theta_h & 0 & \cos\theta_h \end{bmatrix} \begin{Bmatrix} u' \\ v' \\ \omega' \end{Bmatrix} = \mathbf{T} \begin{Bmatrix} u' \\ v' \\ \omega' \end{Bmatrix} \tag{7}$$

Also, we have the following relations:

$$\begin{aligned} x' &= x\cos\theta_h + z\sin\theta_h \\ y' &= y \end{aligned} \tag{8}$$

3. Scattering by Three-Dimensional Topographies

Consider the half-space W_h, see Figure (2). The displacement field related to the half-space is $\mathbf{u_h}$. The traction-free boundary condition applies on the free surface:

$$\mathbf{t_h} = 0 \quad \text{on} \quad \Gamma \tag{9}$$

In W_h, the total displacement $\mathbf{u_h}$ and the total traction $\mathbf{t_h}$ are obtained by applying the principle of superposition as the sum of the free field plus the scattered field:

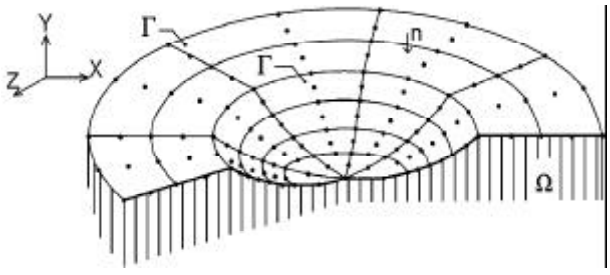

Figure 2. The half-space W_h under the free surface Γ.

$$\mathbf{u_h} = \mathbf{u_s} + \mathbf{u_o}$$
$$\mathbf{t_h} = \mathbf{t_s} + \mathbf{t_o} \tag{10}$$

where the traction $\mathbf{t_o}$ produced by the incident wave can be obtained from:

$$\mathbf{t_o} = \begin{Bmatrix} [(\lambda+2\mu)\frac{\partial u}{\partial x} + \lambda\frac{\partial v}{\partial y} + \lambda\frac{\partial \omega}{\partial z}]n_x + \\ [(\lambda+2\mu)\frac{\partial v}{\partial y} + \lambda\frac{\partial u}{\partial x} + \lambda\frac{\partial \omega}{\partial z}]n_y + \\ [(\lambda+2\mu)\frac{\partial \omega}{\partial z} + \lambda\frac{\partial v}{\partial y} + \lambda\frac{\partial u}{\partial x}]n_z + \\ \mu(\frac{\partial u}{\partial y} + \frac{\partial v}{\partial x})n_y + \mu(\frac{\partial u}{\partial z} + \frac{\partial \omega}{\partial x})n_z \\ \mu(\frac{\partial u}{\partial y} + \frac{\partial v}{\partial x})n_x + \mu(\frac{\partial v}{\partial z} + \frac{\partial \omega}{\partial y})n_z \\ \mu(\frac{\partial u}{\partial z} + \frac{\partial \omega}{\partial x})n_x + \mu(\frac{\partial v}{\partial z} + \frac{\partial \omega}{\partial y})n_y \end{Bmatrix} \tag{11}$$

where n_i is the components of the unit outward normal to the boundary, and the displacements *u*, *v*, and ω are the components of the free field motion $\mathbf{u_o}$ (*u* ,*v* ,ω), given by the expressions (10), (13), (16), and (23) for a harmonic wave propagating in *a* three-dimensional half-space. As the total traction is zero on the boundary Γ, the traction due to the scattered wave can be written as:

$$\mathbf{t_s} = -\mathbf{t_o} \quad \text{on} \quad \Gamma. \tag{12}$$

The displacements and tractions for the half-space due to the scattered wave can be obtained from the following matrix system by using the *BEM*:

$$\mathbf{H_h}\,\mathbf{u_s} - \mathbf{G_h}\,\mathbf{t_s} = 0 \tag{13}$$

in which $\mathbf{G_h}$ and $\mathbf{H_h}$ are the influence matrices obtained from the integration of displacement and traction kernels over the boundary of the half-space, respectively. By applying the traction free boundary condition on Γ, the above equation is written as:

$$\mathbf{H_h}\,\mathbf{u_s} = -\mathbf{G_h}\,\mathbf{t_o} \tag{14}$$

where $\mathbf{u_s}$ is unknown. The total displacements and tractions for the half-space are given by Eq. (10) applying the principle of superposition.

Substituting the scattered values in terms of the total values into Eq. (14), a system of equations with unknowns of total displacements and tractions is obtained:

$$\mathbf{H_h}\mathbf{u_h} = \mathbf{H_h}\mathbf{u_o} - \mathbf{G_h}\mathbf{t_o} \tag{15}$$

4. Comparison with Available Solutions in the Literature

In order to appraise the accuracy and efficiency of the represented formulations for computing the surface displacement amplification, a number of examples are considered. The employed method is based on the *BEM* in the frequency domain. The *BEM* formulations for time-harmonic elastodynamic problems have been presented by Dominguez [39] in full details.

4.1. Hemispherical Canyons

The first results for a hemispherical canyon were published by Sanchez-Sesma [25] for vertical incidence of *P* waves. Afterwards, Eshraghi and Dravinski [21] solved this problem using multipolar expansions of wave functions. Also, Reinoso [40] employed the *BEM* to study this problem.

The shape of this canyon is shown in Figure (3). Material properties of the canyon are $c_1 = \rho = 1$, $\mu = 1/3$, $c_2 = 0.577$, and $\nu = 0.25$, in which ρ is the density, μ is the shear modulus, and ν is the Poisson's ratio. The results obtained by the present method are compared with those of Sanchez-Sesma [25], Eshraghi and Darvinski [21], Reinoso [40] and Sohrabi et al [37] for normalized frequency $\eta_p = .25, .5$ in Figure (4a) and Reinoso [40] for normalized frequencies $\eta_p = .75, 1.5$ in Figure (4b). The dimensionless frequency η_p is introduced as the ratio of the diameter of the canyon and the wavelength of the incident longitudinal wave ($\eta_p = 2a/\lambda = \omega a/c_1\pi$), where ω is the actual frequency of the incident *P* wave and *a* is the radius of the canyon. Our results are drawn with a continuous line, while Reinoso results in Figure (4b) are depicted with filled circles. All of the distances are normalized with respect to the radius of the

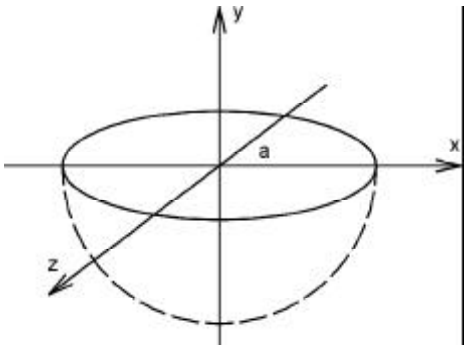

Figure 3. Hemispherical canyon with the radius a.

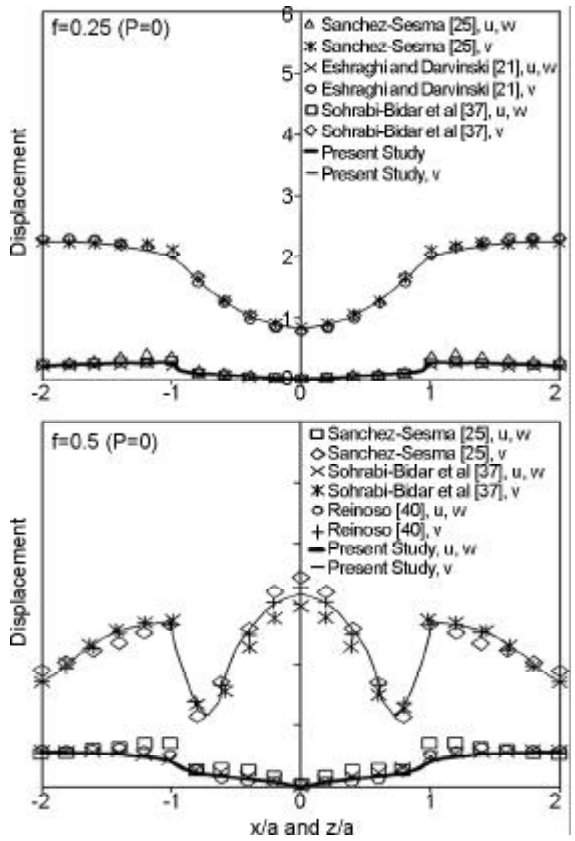

Figure 4a. Amplitude of components of the surface displacement field for a hemispherical canyon due to the vertical incidence of *P* waves with normalized frequencies η_p =.25, .5.

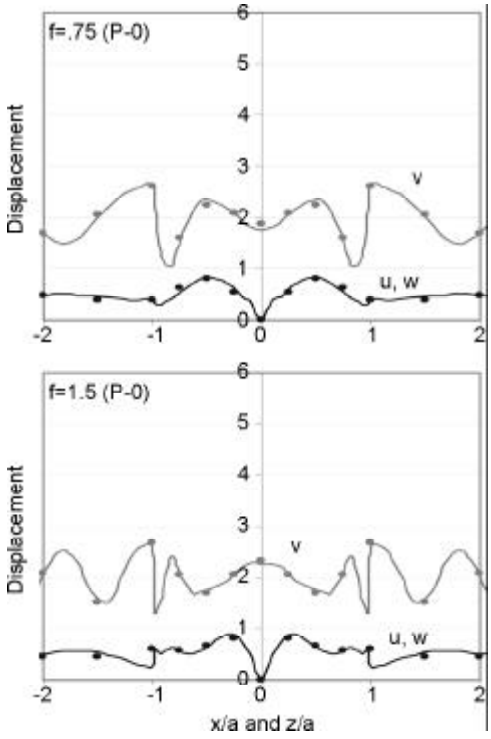

Figure 4b. Amplitude of components of the surface displacement field for a hemispherical canyon due to the vertical incidence of *P* waves with normalized frequencies η_p =.75, 1.5.

canyon. For convenience, all numerical results for the surface displacement field are displayed in terms of the Cartesian components *u*, *v*, and ω. As can be seen, the comparison is satisfactory even for high frequencies. As expected, for vertical incidence of *P* waves, the largest amplification occurs in the vertical component of motion. Also it can be seen that at low frequencies the motion is more even, and by increase of the stimulation frequency it shows more oscillations.

This canyon is also subjected to *SH* and *SV* waves with incidence angles of 0°, 30°, 60° relative to the vertical axis and azimuth of 0°. The following material properties are assumed: $\mu = c_2 = \rho = 1, c_1 = 2,$ $\nu = 1/3$. The comparison of these results with those of Reinoso is presented in Figure (5) for normalized frequency $\eta_s = .75 (\eta_s = \omega\, a / c_2 \pi)$. As expected, in the incidence of *SH* wave only the out-of-plane component of displacement is present in the incident wave plane, while in the case of the incident *SV* wave only the in-plane components of motion are existent. Also, it is observed that for incident *SV* wave the horizontal component *u* is amplified more than the vertical component of motion (i.e. v). This is expected because *SV* waves cause particle to vibrate in the direction perpendicular to the wave propagation path.

4.2. Elliptical-Shaped Canyons

In order to test the accuracy of the present technique for non-axisymmetric geometries, elliptical-shaped canyons are considered which is shown in Figure (6). The results of the present study are compared with those of Eshraghi and Dravinski [21] and Sanchez-Sesma et al [41]. The equation of the semi-ellipsoid is defined by $x^2/a_1^2 + y^2/a_2^2 + z^2/a_3^2 = 1$, $y < 0$ where a_1, a_2, and a_3 are the principal axes of the ellipsoid along the Cartesian coordinates *x*, *y*, and *z*, respectively. In reality, a_1 and a_3 are half of the diameters of the ellipsoid along the *x*- and *z*-directions, respectively, and a_2 is the depth of the canyon. Results are presented for elliptical-shaped canyons with $a_1 \neq a_2 = a_3$. All distances are normalized relative to the half-width of the canyon along the *z*-axis (i.e. a_3). In addition to the actual frequency ω, a dimensionless frequency η_s is defined as the ratio of the diameter of the canyon in the incident wave plane to the wavelength of the incident shear wave. Properties are $c_2 = \rho = \mu = 1$, and *v* = 1/3.

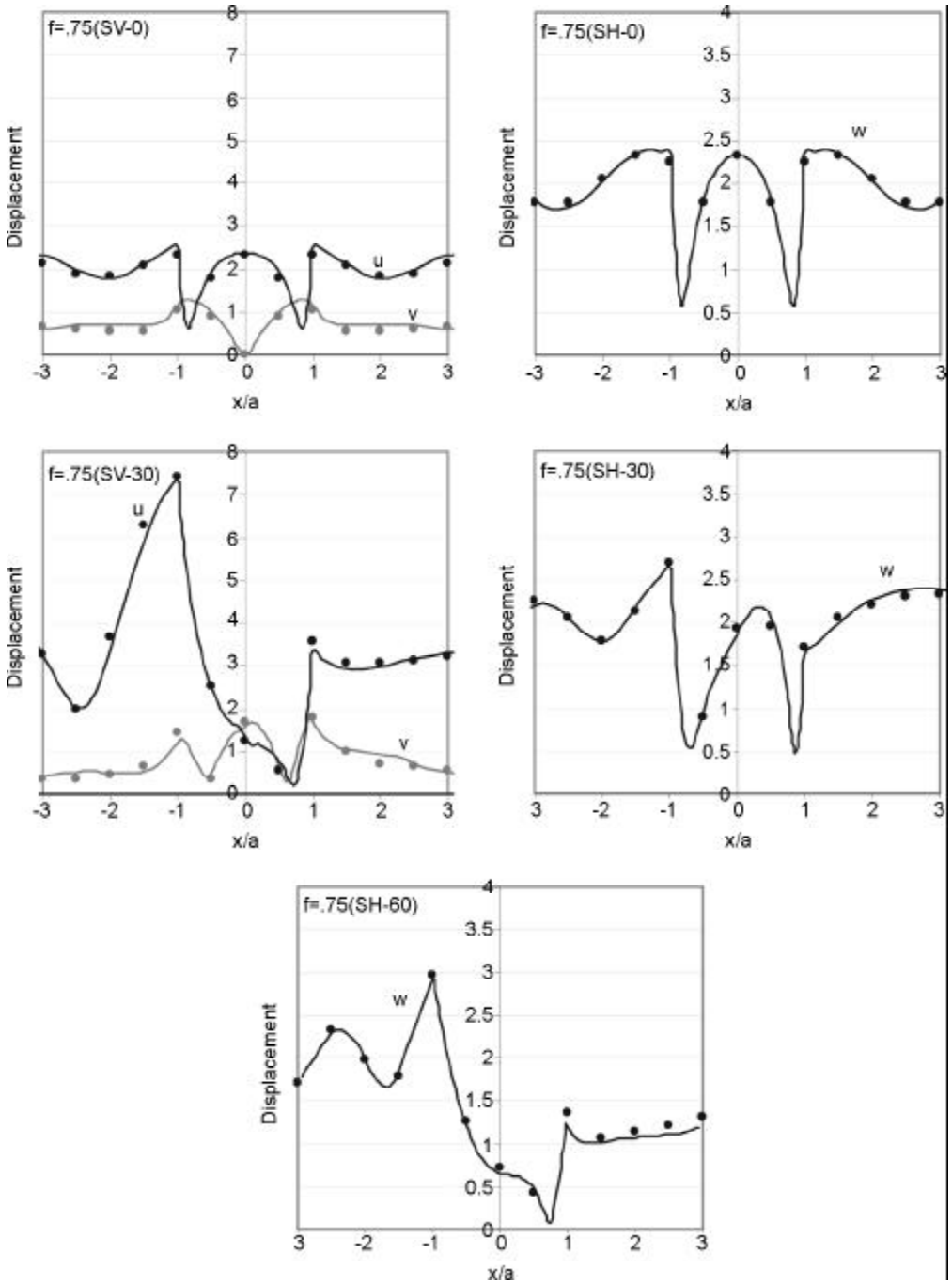

Figure 5. Amplitude of components of the surface displacement field for a hemispherical canyon due to the incident SH and SV waves with incidence angles of 0^o, 30^o, 60^o, horizontal incidence angle 0^o, and normalized frequency $\eta_s = .75$.

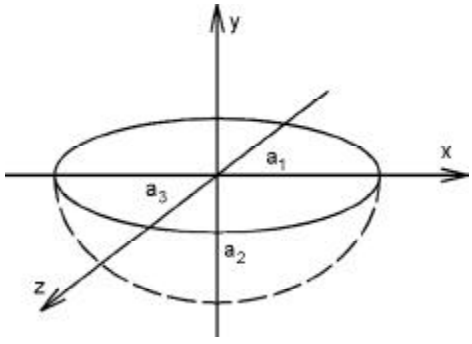

Figure 6. Elliptical-shaped canyon.

Firstly, the canyon is subjected to an incident *P* wave in the *y*-*z* plane (horizontal incidence angle 90°). The dimensions of the axes of this ellipse are 3 and 1, corresponding to the *x*-and *z*-components, respectively; the depth of the canyon is equal to 1($a_1 = 3$, $a_2 = a_3 = 1$). Namely, the shape of the canyon is very elongated. Surface displacement components at stations along the *z*-axis for a normalized frequency $\eta_s = .5$ (relative to a_3) and incidence angles of 0°, 30°, 60° with respect to the *y*-axis are depicted in Figure (7). Because the edges of the canyon in the in-plane direction (propagation wave plane) are much closer to each other than the out-of-plane direction, its response should be close to a two-dimensional approximation of the problem. As expected, these results are very similar to those of the two-dimensional model of the problem, i.e. semicircular canyon with unit radius, shown with filled circles.

Now, an elliptical canyon with $a_1 = 2$, $a_2 = a_3 = 1$ is studied. Results are presented for incident *SH* and *P* waves with three incidence angles, 0°, 30°, 60°, and Rayleigh waves for two azimuth of incidence 0°, 90°. Although the actual frequency of the incident wave is the same for all these incidences, the dimensionless frequency is one (relative to a_1) for an azimuth of incidence 0°, while it reduces to one-half (relative to a_3) for an azimuth of incidence 90°. In all these cases the displacement field is presented for stations along two perpendicular sections of the canyon; in real, the principal axes of the ellipse. In the following figures, the graphs on the left-hand side correspond to the displacement field for stations along the x-axis, and the ones on the right-hand side correspond to stations along the *z*-axis.

For incident *SH* waves, the results for horizontal incidence angles 0°, 90° are presented in Figures (8) and (9), respectively. Similar to the two-dimensional approximation (antiplane strain model), surface displacement field for stations along the *x*-axis, see Figure (8), and the *z*-axis, see Figure (9), only has one component in the *z*- and *x*-directions, respectively. In other words, the motion in the plane of the incident SH wave only occurs in the out-of-plane direction which constitutes the out-of-plane motion. However, for stations along the direction perpendicular to the plane of the incident *SH* wave (*z* in Figure (8) and *x* in Figure (9)), all three components of the displacement field are present except for the vertical incidence which has only two in-plane components of motion. As can be seen, for vertical and oblique incidence of *SH* wave the largest displacement is in the out-of-plane component (*w*-component in Figure (8) and *u*-component in Figure (9)). Apparently, the other two displacement components, non-existent in the two-dimensional approximation, can have substantial amplitudes. Now, the displacement field for stations along the *x*-axis of Figure (8) is compared with the displacement field along the *z*-axis of Figure (9) and vice versa. By comparing the results of Figures (8) and (9), that no drastic change is seen in the pattern and amplitude of the main component of displacement, which is in the out-of-plane direction and is specified in Figures (8) and (9) by the *w*- and *u*-components, respectively, occurs. However, the results for the narrower canyon in the out-of-plane direction (azimuth of incidence 0°) show much larger amplitudes for the two non-principal components of displacement than for the wider canyon (azimuth of incidence 90°). This is expected, because as the edges of the canyon get further apart in the out-of-plane direction, the

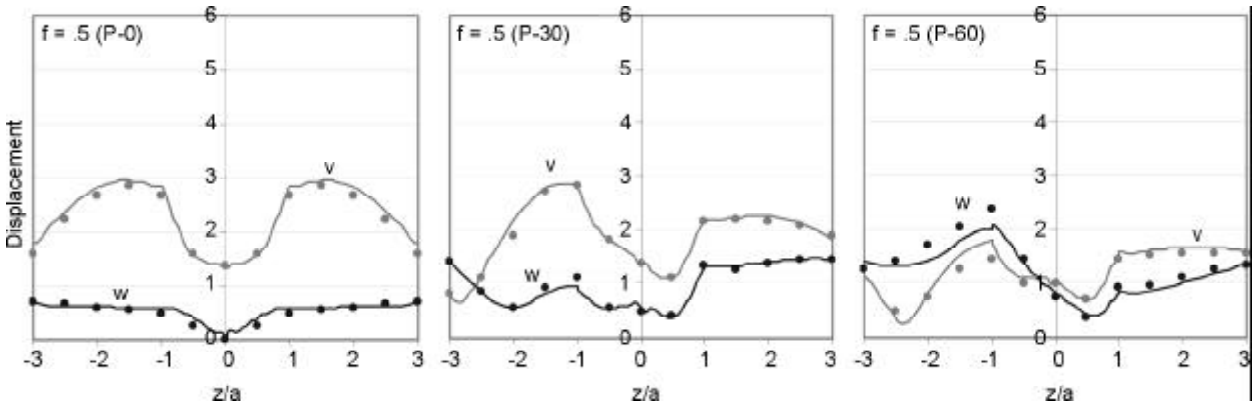

Figure 7. Amplitude of components of the surface displacement field for an elliptical-shaped canyon ($a_1 = 3$, $a_2 = a_3 = 1$) due to the incident *P* wave with incidence angles of 0°, 30°, 60°, horizontal incidence angle 90°, and normalized frequency $\eta_s = .5$.

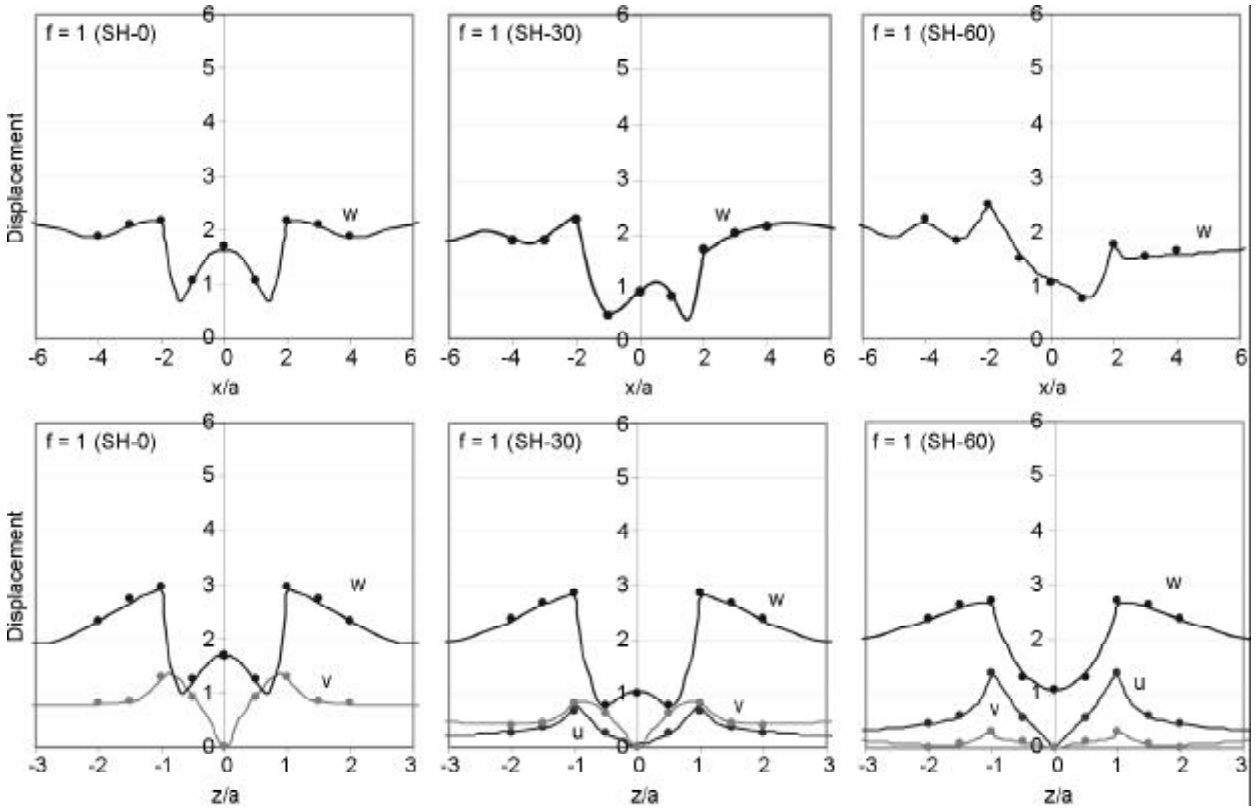

Figure 8. Amplitude of components of the surface displacement field for an elliptical-shaped canyon ($a_1 = 2$, $a_2 = a_3 = 1$) due to the incident SH wave with incidence angles of 0°, 30°, 60°, horizontal incidence angle 0°, and normalized frequency η_s =1.

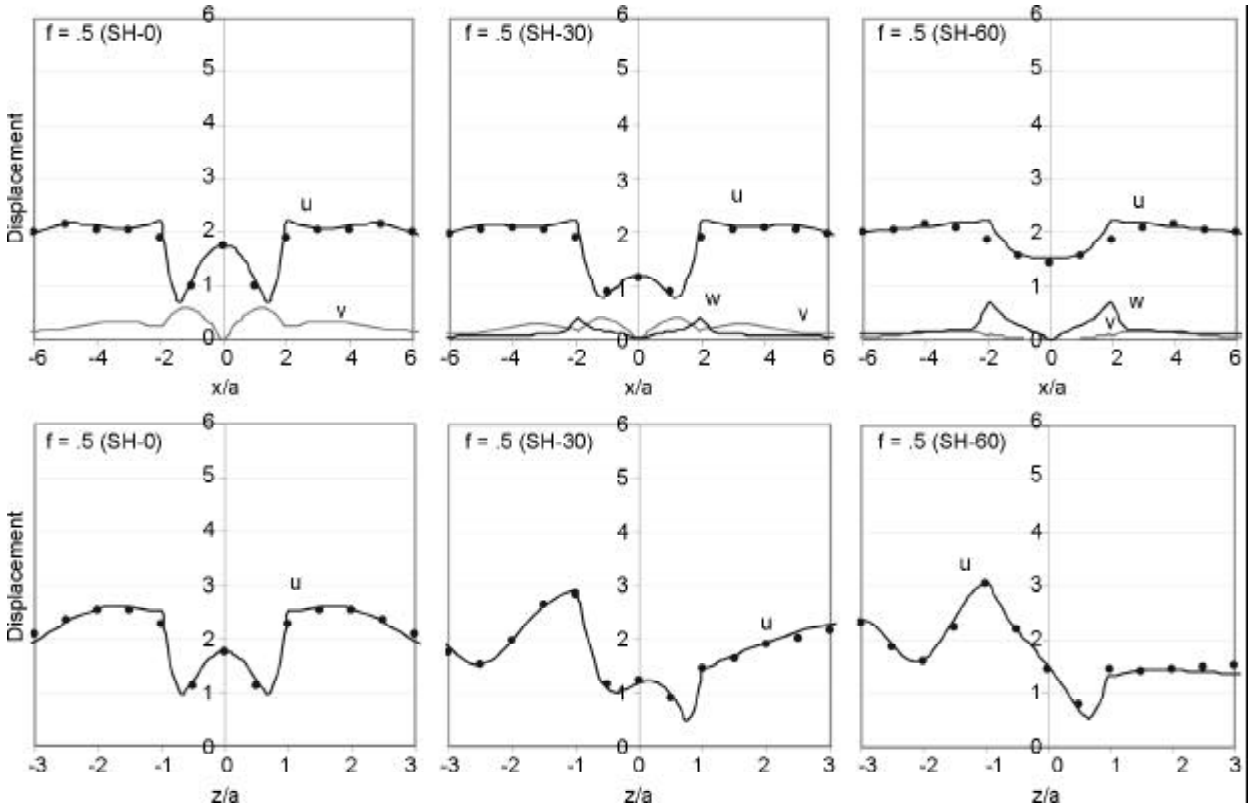

Figure 9. Amplitude of components of the surface displacement field for an elliptical-shaped canyon ($a_1 = 2$, $a_2 = a_3 = 1$) due to the incident SH wave with incidence angles of 0°, 30°, 60°, horizontal incidence angle 90°, and normalized frequency η_s =.5.

model approaches further and further to a cylindrical geometry, where the two non-principal components of displacement are non-existent.

Figures (10) and (11) correspond to incident *P* waves with horizontal incidence angles 0^o and 90^o, respectively. Similarly to the two-dimensional

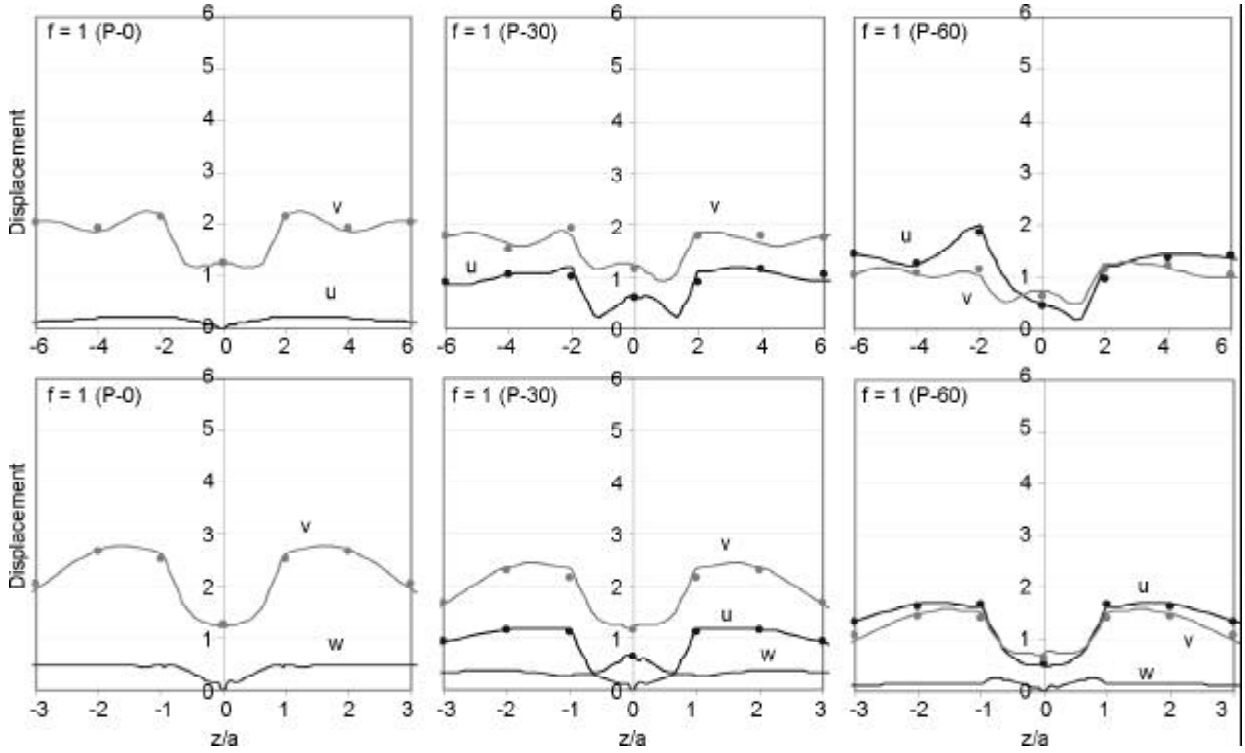

Figure 10. Amplitude of components of the surface displacement field for an elliptical-shaped canyon ($a_1 = 2$, $a_2 = a_3 = 1$) due to the incident *P* wave with incidence angles of 0^o, 30^o, 60^o, horizontal incidence angle 0^o, and normalized frequency η_s =1.

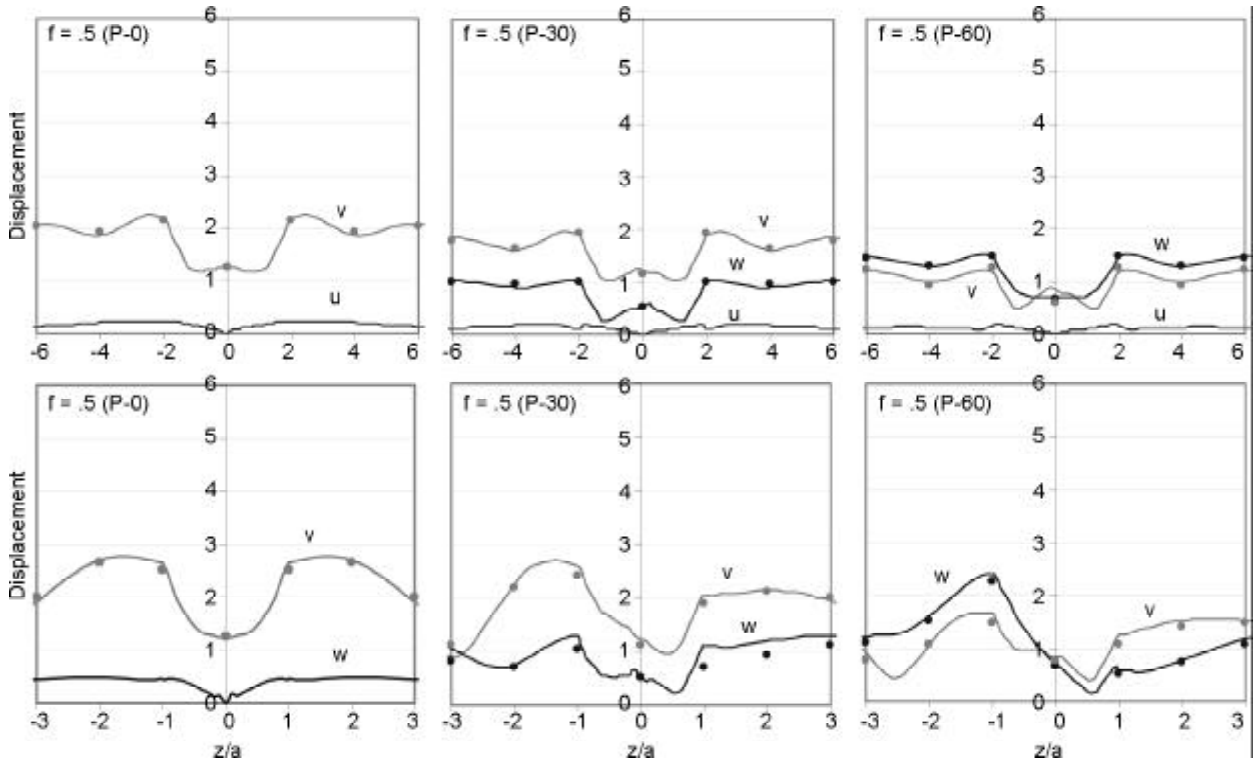

Figure 11. Amplitude of components of the surface displacement field for an elliptical-shaped canyon ($a_1 = 2$, $a_2 = a_3 = 1$) due to the incident *P* wave with incidence angles of 0^o, 30^o, 60^o, horizontal incidence angle 90^o, and normalized frequency η_s =.5.

approximation, for stations along the in-plane direction the displacement field consists only of two components which constitute the in-plane motion. However, for stations along the out-of-plane direction an additional component of displacement field appears for oblique incidences, which are due to the 3*D* scattering. It is observed that the two in-plane components of displacement (*u* and *v* in Figure (10) display characteristics similar to those of their counterparts (*w* and *v* in Figure (11)). As expected, for vertical incidence of *P* waves the results are independent of the azimuth of incidence, so for all horizontal angles the same results are obtained.

Figures (12) and (13) show the responses for incident Rayleigh waves with azimuth of incidence 0^o and 90^o, respectively. Analogously to the two-dimensional approximation, in the in-plane direction only the two in-plane components of motion can be produced, while in the out-of-plane direction the scattering of the canyon produces displacements in all directions.

These results demonstrate that a change in the azimuth of incidence may greatly affect the surface displacement field. This observation emphasizes the need for three-dimensional modeling of actual surface irregularities since two-dimensional approximations may result in a poor assessment of the real displacement field.

5. Study of a Surface Topography

5.1. Hemispherical Hills

In this problem, a hemispherical hill of radius *a* is considered which is shown in Figure (14). The material properties of the hill are assumed to be equal to those of the hemispherical canyon in order to make reasonable comparisons.

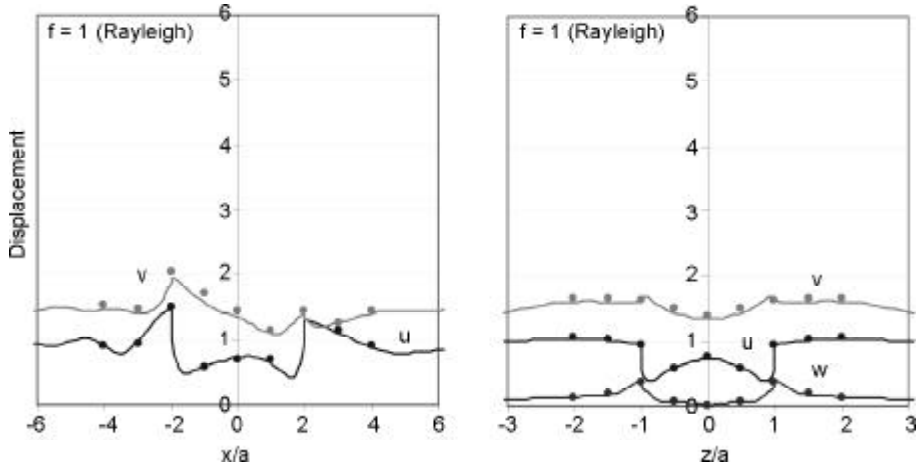

Figure 12. Amplitude of components of the surface displacement field for an elliptical-shaped canyon ($a_1 = 2$, $a_2 = a_3 = 1$) due to the incident Rayleigh wave with horizontal incidence angle 0^o, and normalized frequency $\eta_s = 1$.

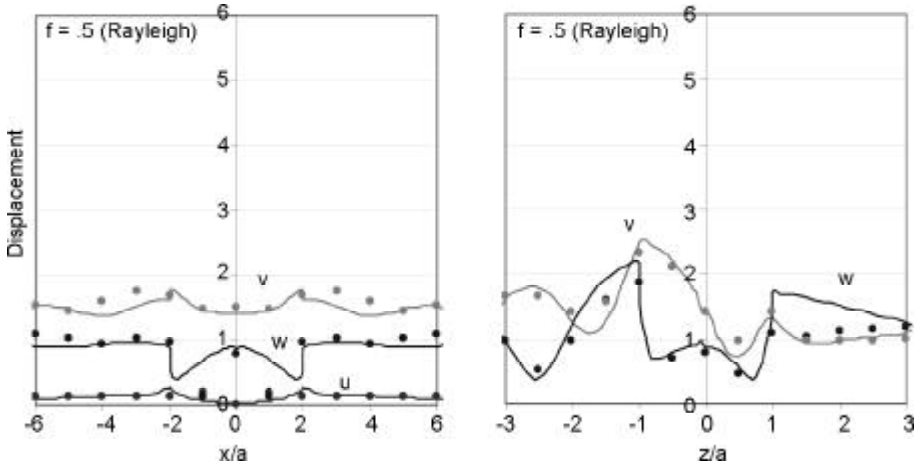

Figure 13. Amplitude of components of the surface displacement field for an elliptical-shaped canyon ($a_1 = 2$, $a_2 = a_3 = 1$) due to the incident Rayleigh wave with horizontal incidence angle 90^o, and normalized frequency $\eta_s = .5$.

The response of this topography due to the vertical incidence of *P* waves is shown in Figure (15) for normalized frequencies $\eta_s = .25, .5, .75, 1.5$. As observed again, by increase of the stimulation frequency the motion shows more oscillations. It can be seen that the amplifications are generally larger than those made by the hemispherical canyon. Also, the site amplification results of the hemispherical hills have the same pattern with the results of reference [37] for gaussian hills subjected to incidence of *P* waves.

5.2. Rectangular Cube Canyons

In order to study the effect of shape and depth of the canyon in amplification of the earthquake waves, rectangular cubic canyons are considered as shown in Figure (16). The dimension of these canyons in the horizontal surface are 2×2 and the depth of them are $H = 0.5, 1, 1.5, 2$. The material properties of the canyons are assumed to be equal to those of the hemispherical canyon and hemispherical hill. The surface displacement of these canyons for vertical incidence of *P* wave in normalized frequency of $\eta_p = .25$ is shown in Figure (17).

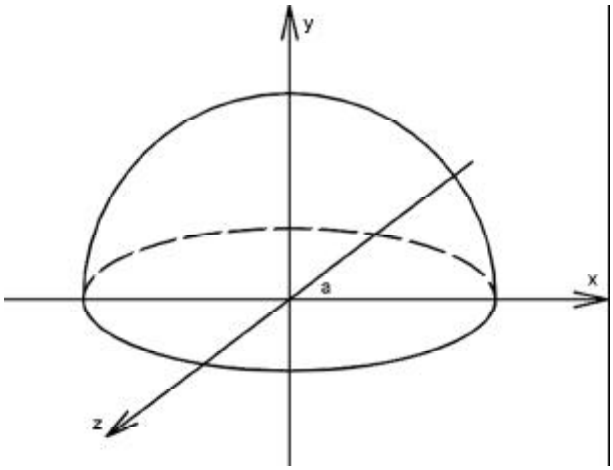

Figure 14. Hemispherical hill with the radious a.

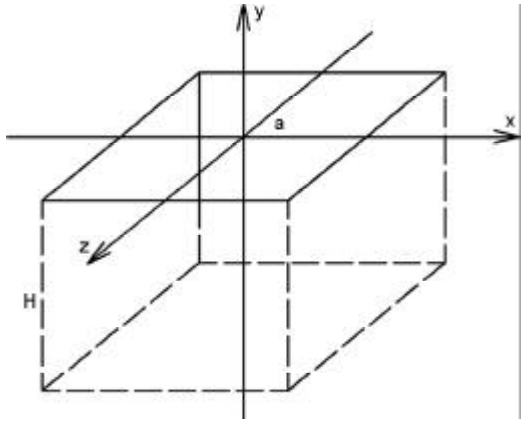

Figure 16. Rectangular cube canyon with the depth of H.

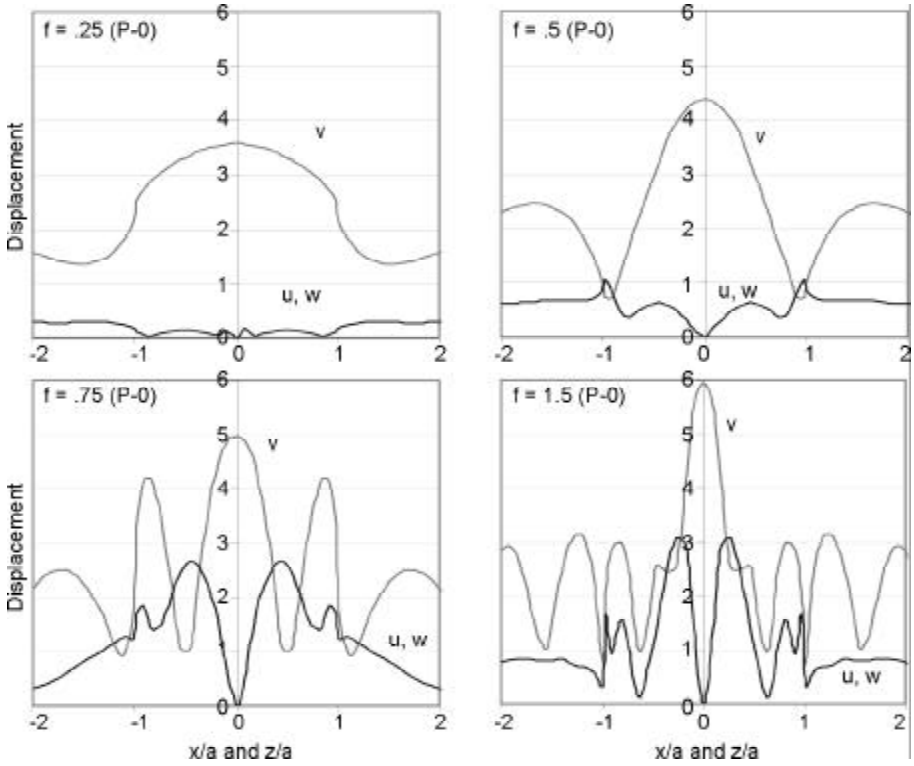

Figure 15. Amplitude of components of the surface displacement field for a hemispherical fill due to the vertical incident *P* waves with normalized frequencies $\eta_p = .25, .5, .75, 1.5$.

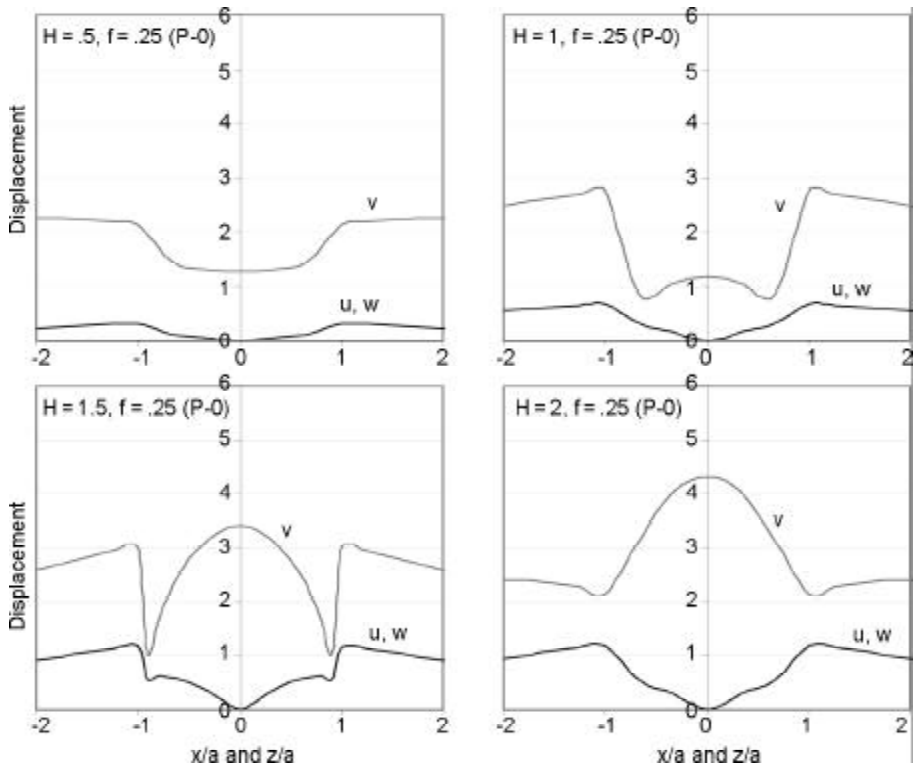

Figure 17. Amplitude of components of the surface displacement field for a rectangular cube canyon with depth of H = 0.5, 1, 1.5, 2 for the vertical incidence of P wave in normalized frequency η_p = 2.5.

6. Conclusions

The behavior of irregularities such as hemispherical canyons, elliptical shaped canyons, hemispherical hills and rectangular cube canyons subjected to various waves with different incident angles are all investigated in the paper. The results of the hemispherical and elliptical shaped canyons are compared with the available studies with different approaches. The effect of the different canyon depths and different frequency of incident waves are also investigated in the parametric study of the two last examples. The influence of the other effective factors such as surface topography type, frequency of incident waves, azimuth and angle of incidence are all investigate quantitavely so as to gain insight to the problem. Such an integrated study of topographic effects using *BEM* is not available in the other works. The comparative study showed the validity and limitation of the corresponding two-dimensional approximations (antiplane models). Results apparently indicate that, in general, the dimensions of the site under consideration suggest the suitable approach. As a case in point, when the edges of the canyon in the out-of-plane direction (with respect to the incident wave plane) are close to each other, the three-dimensional nature of the problem becomes more prominent, and it cannot be modeled by two-dimensional approximations. It can be realized that in incidence where the propagation wave path is perpendicular or almost perpendicular to the inclination wall, the motion tends to be more amplified than the case where incidence takes place parallel to the slope. Also, graphs are representative of amplification factor as a function of the topography coordinates. From the numerical aspects of the solution, it is concluded that in order to provide acceptable convergence, as the frequency of the incident wave or its incidence angle relative to the vertical axis increases, the length of the discretization over the free surface of the half space must increase as well.

Finally, the main conclusion of the paper based on the comparative and parametric studies of the investigated problems is that a realistic and complete study of site effects on surface ground motion amplification in the above mentioned situations requires three-dimensional modeling of irregularities. In addition, surface topography, incident wave type, related frequency, and azimuth and angle of incidence must be considered in site effect studies.

References

1. Anderson, J.G., Bodin, P., Brune, J.N., Prince, J., Singh, S.K., Quaas, R., and Onate, M. (1986). "Strong Ground Motion from the Michoacan, Mexico Earthquake", *Science*, **233**, 1043-1049.

2. Dravinski, M. and Mossessian, T.K. (1987). "Scattering of Harmonic P, SV and Rayleigh Waves by Dipping Layers of Arbitrary Shape", Bull. Seism. Soc. Am., 77, 212-235.

3. Trifunac, M.D. and Hudson, D.E. (1971). "Analysis of the Pacoima Dam Accelerogram San-Fernando, California, Earthquake of 1971", Bull. Seism. Soc. Am., **61**, 1393-1411.

4. Boore, D.M. (1973). "The Effect of Simple Topography on Seismic Waves: Implications for Accelerations Recorded at Pacoima Dam, San-Fernando Valley, California", Bull. Seism. Soc. Am., **63**, 1603-1609.

5. Davis, L.L. and West, L.R. (1973). "Observed Effects of Topography on Ground Motion", Bull. Seism. Soc. Am., **63**, 283-298.

6. Esquivel, J.A. and Sanchez-Sesma, F.J. (1980). "Effects of Canyon Topography on Dynamic Soil-Bridge Interaction for Incident Plane SH Waves", *Proc. 7th World Conf. Earthquake Eng.*, Istanbul, **2**, 153-160.

7. Trifunac, M.D. (1973). "Scattering of Plane SH-Waves by a Semicylindrical Canyon", *Earth. Eng. Struct. Dyn.*, **1**(2), 67-81.

8. Wong, H.L. and Trifunac, M.D. (1974). "Scattering of Plane SH-Waves by a Semi-Elliptical Canyon", *Earth. Eng. Struct. Dyn.*, **1**, 57-69.

9. Wong, H.L. and Jennings, P.C. (1975). "Effect of Canyon Topographies on Strong Ground Motion", Bull. Seism. Soc. Am., **65**(12), 39-57.

10. Sabina, F.J. and Willis, J.R. (1975). "Scattering of SH-Waves by a Rough Half-Space of Arbitrary Shape", *Geophys. J.*, **42**, 685-703.

11. Sanchez-Sesma, F.J. and Rosenblueth, E. (1979). "Ground Motion at Canyons of Arbitrary Shapes under Incident SH-Waves", *Earth. Eng. Struct. Dyn.*, **7**(4), 41-50.

12. Lee, V.W. (1982). "A Note on the Scattering of Elastic Plane Waves by a Hemispherical Canyon", *Soil Dyn. Earth. Eng.*, **1**, 122-129.

13. Moeen-Vaziri, N. and Trifunac, M.D. (1985). "Scattering of Plane SH-Waves by Cylindrical Canals of Arbitrary Shape", *Soil Dyn. Earth. Eng.*, **4**, 18-23.

14. Sanchez-Sesma, F.J. (1987). "Sites Effects on Strong Ground Motion", *Soil Dyn. Earth. Eng.*, **6**, 124-132.

15. Mossessian, T.K. and Dravinski, M. (1987). "Application of a Hybrid Method for Scattering of P, SV and Rayleigh Waves by Near Irregularities", Bull. Seism. Soc. Am., **77**(1), 784-803.

16. Luco, J.E., Wong, H.L., and de Barros, F.C.P. (1990). "Three Dimensional Response of a Cylindrical Canyon in a Layered Half-Space", *Earth. Eng. Struct. Dyn.*, **19**, 799-817.

17. Chongbin, Z. and Valliappan, S. (1992). "Effect of Canyon Topographic Conditions on Ground Motion Due to P and SV Wave Incidences", *Proc. 10th World Conference on Earthquake Engineering*, Madrid, Spain, 923-928.

18. Geli, L., Bard, P.Y., and Jullien, B. (1988). "The Effect of Topography on Earthquake Ground Motion: A Review and New Results", Bull. Seism. Soc. Am., **75**, 42-63.

19. Sanchez-Sesma, F.J., Bravo, M.A., and Herrera, I. (1985). "Surface Motion of Topographical Irregularities for Incident P, SV and Rayleigh Waves", Bull. Seism. Soc. Am., **75**, 263-269.

20. Wong, H.L. (1982). "Effect of Surface Topography on the Diffraction of P, SV and Rayleigh Waves", Bull. Seism. Soc. Am., **72**(11), 67-83.

21. Eshraghi, H. and Dravinski, M. (1989). "Scattering of Plane Harmonic SH, SV, P and Rayleigh Waves by Non-Axisymmetric Three-Dimensional Canyons: A Wave Function Approach", *Earth. Eng. Struct. Dyn.*, **18**(9), 83-98.

22. Kawase, H. (1988). "Time-Domain Response of a Semi-Circular Canyon for Incident SV, P and Rayleigh Waves Calculated by the Discrete Wave Number Boundary Element Method", Bull. Seism. Soc. Am., **78**(14), 15-37.

23. Chuhan, Z. and Chongbin, Z. (1988). "Effects of Canyon Topography and Geologic Conditions on Strong Ground Motion", *Earth. Eng. Struct. Dyn.*, **16**, 81-97.

24. Lee, V.W. (1978). "Displacement Near a Three-Dimensional Hemispherical Canyon Subjected to Incident Plane Waves", Univ. of Southern California, Dept. of Civil Engineering, Report No.78-16

25. Sanchez-Sesma, F.J. (1983). "Diffraction of Elastic Waves by Three-Dimensional Surface Irregularities", Bull. Seism. Soc. Am., **73**, 1621-1636.

26. Sneider, R. (1986). "The Influence of Topography on the Propagation and Scattering of Surface Waves", *Phys. Earth Planet. Inter 444*, 226-241.

27. Mossessian, T.K. and Dravinski, M. (1989). "Scattering of Elastic Waves by Three- Dimensional Surface Topographies", Wave Motion, North-Holland, 579-592.

28. Reinoso, E., Wrobel, L.C., and Power, H. (1996). "Three-Dimensional Scattering of Seismic Waves from Topographical Structures", *Soil Dynamics and Earthquake Engineering*, Elsevier Science Limited Printed in Great Britain, 41-61.

29. Omidvar, B., Rahimian, M., Mohammadnejad, T., and Sanaeiha, A. (2010). "Three-Dimensional Scattering of Plane Harmonic SH, SV, and P Waves in Multilayered Alluvial Valleys", *Asian Journal of Civil Engineering (Building and Housing)*, **11**(5), 605-626.

30. Gatmiri, B., Arson, C., and Nguyen, K.V. (2008). "Seismic Site Effects by an Optimized 2D BE/FE Method I. Theory, Numerical Optimization and Application to Topographical Irregularities", *Soil Dynamics and Earthquake Engineering*, **28**, 632-645.

31. Gatmiri, B. and Arson, C. (2008). "Seismic Site Effects by an Optimized 2D BE/FE Method II. Quantification of Site Effects in Two-Dimensional Sedimentary Valleys", *Soil Dynamics and Earthquake Engineering*, **28**, 646-661.

32. Kamalian, M., Gatmiri, B., and Sohrabi-Bidar, A. (2003). "On Time-Domain Two-Dimensional Site Response Analysis of Topographic Structures by BEM", *J. of Seismology and Earthquake Engineering*, **5**, 35-45.

33. Kamalian, M., Jafari M.K., Sohrabi-Bidar, A., Razmkhah A., and Gatmiri, B. (2006a). "Time-Domain Two-Dimensional Site Response Analysis of Non-Homogeneous Topographic Structures by a Hybrid FE/BE Method", *Soil Dynamics and Earthquake Engineering*, **26**, 753-765.

34. Kamalian, M., Gatmiri, B., Sohrabi-Bidar, A., and Khalaj, A. (2007a). "Amplification Pattern of 2D Semi-Sine Shaped Valleys Subjected to Vertically Propagating Incident Waves", Communication in Numerical Methods in Engineering, **23**, 871-887.

35. Kamalian, M., Jafari, M.K., Sohrabi-Bidar, A., and Razmkhah, A. (2008a). "Seismic Response of 2D Semi-Sine Shaped Hills to Vertically Propagating Incident Waves: Amplification Patterns and Engineering Applications", *Earthquake Spectra*, **24**, 405-430.

36. Kamalian, M., Sohrabi-Bidar, A., Razmkhah A., Taghavi, A., and Rahmani, I. (2008b). "Considerations on Seismic Microzonation in Areas with Two-Dimension Hills", *Journal of Earth System Science*, **117**, 783-796.

37. Sohrabi-Bidar, A., Kamalian, M., and Jafari, M.K. (2009). "Time-domain BEM for Three-Dimensional Site Response Analysis of Topographic Structures", *Int. Journal of Numerical Methods Engineering*, **79**, 1467-1492.

38. Lee, Sh.J., Komatitsch, D., Huang, B.Sh., and Tromp, J. (2009). "Effects of Topography on Seismic-Wave Propagation: An Example from Northern Taiwan", Bulletin of the Seismological Society of America, **99**(1), 314-325.

39. Dominguez, J. (1993). "Boundary Elements in Dynamics", Computational Mechanics Publications.

40. Reinoso, E. (2002). "Scattering of Seismic Waves: Applications to the Mexico City Valley", Computational Mechanics Publications.

41. Sanchez-Sesma, F.J., Perez-Rocha, L.E., and Chavez-Perez, S. (1989). "Diffraction of Elastic Waves by 3D Surface Irregularities", Part II, Bull. Seism. Soc. Am., **19**, 101-112.